# FEDSM-ICNMM2010-30859

# EXPERIMENTAL MEASUREMENT OF PRESSURE PULSES FROM A PULP SCREEN ROTOR

**Sean Delfel**
Pulp and Paper Centre and Department of Mechanical Engineering, The University of British Columbia
Vancouver, BC, Canada

**James Olson**
Pulp and Paper Centre and Department of Mechanical Engineering, The University of British Columbia
Vancouver, BC, Canada

**Carl Ollivier-Gooch**
Department of Mechanical Engineering, The University of British Columbia
Vancouver, BC, Canada

**Phil Wallace**
Pulp and Paper Centre and Department of Mechanical Engineering, The University of British Columbia
Vancouver, BC, Canada

## ABSTRACT

Pressure screens are the most industrially effective way to remove contaminants from a pulp stream, improving the strength, smoothness, and optical qualities of both new and recycled paper. Pressure screens are comprised of two main components: a screen cylinder with narrow slots or small holes and a rotor. The main function of the rotor is to prevent the narrow cylinder apertures from becoming plugged by pulp and debris. In this study, the pressure pulses generated by a novel multi-element foil (MEF) and a single-element foil rotor in a pressure screen were measured at various foil configurations, rotor speeds, and flow rates. The experimental measurements were compared to the results from a computational fluid dynamics model (CFD). Experimental measurements showed that increasing both the angle-of-attack and the flap angle of the MEF increases the magnitude of the negative pressure pulse and reduce the magnitude of the maximum pressure pulse generated by the rotor. At the optimum configurations, the MEF was shown to produce a 126% higher magnitude negative pressure pulse and a 39% lower magnitude positive pressure pulse. It was also found that at higher tip speeds the magnitude of the pressure pulse varies with tip speed squared and the non-dimensional pressure coefficient is Reynolds number independent. Similarly, at higher tip speeds increasing the velocity of the flow through the slots had no effect on the pressure pulse generated by the rotor. At lower rotor speeds, however, the dimensionless pressure was increasingly depending on Reynolds number as slot flow velocity was increased. This is likely due to the increase in slot flow velocity causing the onset of flow separation over the foil. Finally, the numerical model was shown to accurately predict the pressure pulses generated by the MEF at low angles-of-attack and flap angles. However, the model predicted that the foil would stall at lower
angles than what was shown experimentally. This is probably because the CFD model used a solid wall boundary condition rather than modeling the slots in the cylinder, preventing low momentum fluid from re-entering the domain.

## INTRODUCTION

Pressure screens are the most industrially effective way to remove contaminants from a pulp stream, improving the strength, smoothness, and optical qualities of the paper. Pressure screens are also used to fractionate the pulp stream, separating the fibers by length for differing processing and the development of high value pulp products.

Pressure screens, as illustrated in Figure 1, are comprised of two main components: a screen cylinder with narrow slots or small holes and a rotor. The unscreened pulp enters the screen tangentially via a feed stream and passes into the center of the cylinder. Fibres pass through the apertures in the cylinder into the accept stream while oversized debris passes down the length of the screen and exits through the reject port. Pulp fibres are typically 0.02-0.04 mm in diameter and 1-2 mm in length, while the slots in cylinder are on the order of 0.1 mm in width. In order to prevent the small apertures in the cylinder from plugging with fibres and debris, the rotor spins inside the cylinder, generating negative pressure pulses at the cylinder surface that backflush the flow through the apertures, clearing them of debris (1-4).

Previous studies have shown that the magnitude of the pressure pulses generated by the rotor directly affects the capacity of the screen (5-11). It has also been shown that the non-dimensional pressure coefficient is Reynolds number independent, where the pressure coefficient $C_P$ is defined as

$$C_P = \frac{P}{(1/2)\rho V_t^2} \qquad [1]$$

$P$ is the static pressure, $\rho$ is the fluid density, and $V_t$ is the tip speed of the rotor (4, 12). Reynolds number $Re$ is defined as

$$Re = \frac{\rho V_t c}{\mu} \qquad [2]$$

where $c$ is the foil chord length and $\mu$ is the dynamic viscosity of the fluid. This means that for fully turbulent flow the magnitude of the pressure pulses generated by the rotor is proportional to the tip speed squared.
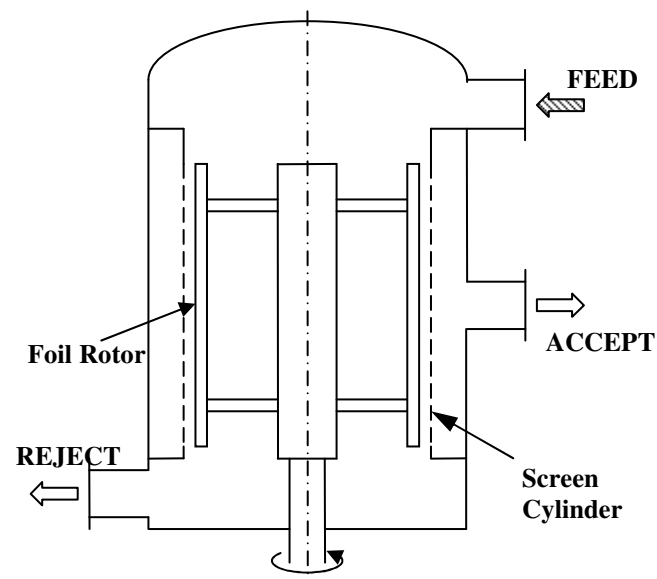


**Figure 1: An Illustration of a Modern Pressure Screen.**

Previous studies also found that the power consumption of the rotor is proportional to the tip speed of the rotor cubed, and that the non-dimensional power coefficient is also Reynolds number independent (13). The power coefficient $C_{Power}$ is defined as

$$C_{Power} = \frac{Power}{\rho V_t^3 D^2} \qquad [3]$$

where *Power* is the power consumption of the rotor and $D$ is the diameter of the rotor. By maximizing the magnitude of the $C_P$ generated by the rotor, the rotor can be slowed, reducing power consumption without reducing the maximum capacity of the screen. This is the primary goal in pressure screen rotor design.

There have been a number of studies experimentally investigating the pressure pulses generated by a pressure screen rotor. Yu studied the pressure pulses from a single S-type solid core rotor for a range of tip speeds and flow rates

(14). It was observed that the pressure pulses were not affected by increasing flow rates, although the tip speeds studied were all fairly high (15 m/s to 25 m/s). Recently, Atkins studied the effects of flow rate, tip speed, and consistency on the pressure pulses generated by a foil rotor and a solid core step rotor (15). It was found that, with water, increasing reject rate $R_V$ at a constant feed flow rate (i.e. increasing accept flow while reducing reject flow) had no effect on the pressure pulse below $R_V = 0.3$ for either the step rotor or foil rotor. Increasing the feed flow caused the magnitude of the pressure pulse generated by the foil rotor to increase, however. No explanation was offered for this phenomenon. Atkins also found that varying consistency between 0.0% and 2.8% had little effect on the pressure pulse for both rotors. While insightful, neither study thoroughly investigated the combined effects of rotor geometry and slot velocity on the pressure pulses generated.

Previous works have also established computational fluid dynamics (CFD) as a useful tool in the study of pressure screen rotors. Karvinen and Halonen made early attempts at validating CFD for use with pressure screen rotors, and achieved good results for the time (16). Wikstrom studied numerically the pressure pulses generated by two separate rotor shapes (17). Atkins used a 3-D CFD model to study the pulses from a single solid core rotor and found very good agreement with experimental results (15). Recent studies have also used CFD to optimize the shape of the rotor elements (3, 18, 19).

The effect of varying the geometry of the element shape on the pressure pulse from a foil rotor was investigated by Gonzales experimentally and Feng *et al.* numerically, using CFD (3, 4). The apparatus used by Gonzales was a small, laboratory "cross-sectional screen", which represented a thin, 2 in. slice of a pressure screen and had no accept flow near the sensor. They found that increasing the camber, or curvature, of the foil greatly increased both the width and magnitude of the pressure pulse. They also showed that increasing the angle-of-attack $\alpha$ of the foil, defined as the angle of the foil with the tangent line, increased the magnitude of the negative portion of the pressure pulse while at the same time reducing the undesirable positive portion of the pressure pulse. Positive pressure pulses are undesirable because they would, at best, push debris retained by the screen through to the accept stream and, at worst, cause the apertures to further plug. Similar observations were made by Niinimaki, who showed that increasing the foil angle-of-attack improves the maximum capacity of the screen (6). Beyond a certain angle-of-attack, however, Gonzales and Feng *et al.* found the foil would begin to stall and the magnitude of the pressure pulse would diminish. This was especially true for highly cambered foils, which would stall at very low angles-of-attack (3, 4).

In order to achieve higher angles-of-attack with highly cambered foils without flow separation, a multi-element foil (MEF) rotor was designed using CFD (19). The multi-element foil, similar in concept to flaps on an airplane, was shown to delay the foil from stalling by allowing high energy flow on the lower surface of the foil to pass through the slot between the main foil and flap, reenergizing the boundary

layer over the upper surface of the foil. The MEF, shown in Figure 2, was also shown to have the added benefit of effectively increasing the camber of the foil by deflecting the flap. This led to a significant increase in the magnitude of the negative pressure pulse generated by the foil compared to a typical single-element rotor foil. The MEF was tested in pilot plant and mill trials, and was shown to be capable of lowering the rotor power consumption significantly, by operating at
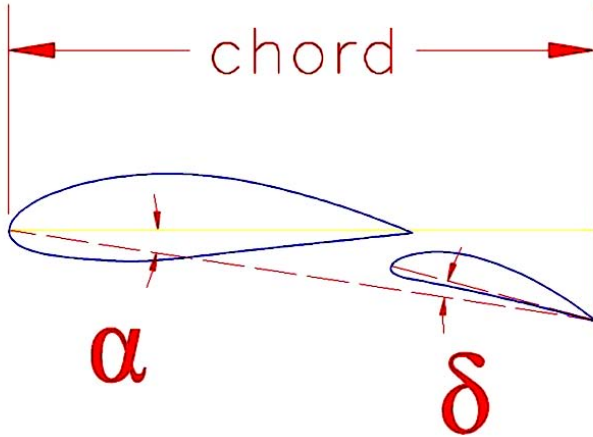


*Figure 2: Cross Section of the MEF with Angle-of-Attack (α), Flap Angle (δ), and Chord Length Defined.*

lower tip speeds, without affecting screen capacity (20, 21). In addition to increased industrial performance, the MEF has been shown to be useful in research applications due to the ability to easily study the effects of foil geometry by changing the angle-of-attack and flap angle.

In an effort to further investigate the effectiveness of multi-element foil pressure screen rotors and to more generally provide insight for and improve upon pressure screen rotor design, this study directly measures the pressure pulses generated by foil rotors in a true screening environment using a laboratory pressure screen. The effect of varying foil geometry on the pressure pulses is studied using 12 different MEF configurations and a single-element foil rotor, representing the current state of the art. Additionally, the effects of rotor tip speed and slot velocity on the pressure pulses are also studied. Finally, the effectiveness of CFD models used in recent pressure screen studies (1-3, 15, 19) are investigated by comparing CFD predictions of pressure with experimental measurements for the MEF rotor.

## EXPERIMENTAL SETUP

A Belloit MR-8 laboratory pressure screen was used in the study, shown in Figure 3. The MR-8 is 8 in. (20.32 cm) in diameter and is equipped with a variable frequency drive (VFD) that allows for control of the rotor speed and power measurements. The screen is also equipped with magnetic flow meters on the accept and reject lines, and pressure sensors on the feed, accept, and reject pipes. The screen is fed from a 1,000 L stock tank, with the accept and reject streams recirculating back into the feed tank. Water (0.0% consistency) was used in the experiment for a number of reasons.

The pressure pulses generated by the rotor were measured using an Entran EPX micro-sensor. The sensor diaphragm has a diameter of 0.15 in. and was installed with the diaphragm flush with the feed side of a wedge-wire cylinder with a 0.15 mm slot width. The sensor was installed so that only a portion of a single wire and two slots are affected. The sensor was installed half way down the axial distance of the cylinder in order to avoid any unsteadiness in the flow as it enters and exits the cylinder. Atkins and Yu both observed a reduction in the strength of the pressure pulses generated by the rotor as the flow moves axially down the cylinder (14, 15). This is likely due to a reduction in the velocity of the flow relative to the rotor as the flow is accelerated by drag from the rotor. By placing the sensor at the axial midpoint, it is the intention to capture the pressure pulse at a point where the flow is fully developed and a steady swirl velocity has been achieved.

The pressure sensor signal was captured at 100k samples per second. At the highest tip speed studied ($V_t$ = 15 m/s), this amounts to 3,937 samples per revolution. The samples were collected continuously and then split into individual pulses for each foil in post-processing. This was done to account for any physical differences between the two foils on the rotor, including differences in gap or manufacturing defects. Additionally, as done in previous studies (1-4, 14, 15, 18, 19), the data was zeroed to a freestream value to isolate the pressure pulses from the rotor from any pressure variations caused by changing flow rates. The average pressure half way between each of the two pulses was used for this value. Because the flow in the screen is turbulent, it was necessary to generate an ensemble average of the pulses. In building the ensemble average a minimum of 500 pulses from each foil was collected. When averaged, the minimum values for each pulse were aligned to prevent any loss in the magnitude of the pulse due to small errors or fluctuations in rotor speed during the sampling period.

Thirteen separate rotors were tested in the study: twelve MEF configurations and a single-element foil (AFT EP) rotor. Table 1 shows the specific MEF geometries studied and the test parameters. The angle-of-attack ($α$) of the MEF was varied between zero and six deg., and the flap angle ($δ$) was varied between 12 and 22 deg. The angles of the foils are set by CNC milled end plates in order to reduce errors in the geometry. The MEF and the EP used both have chord lengths of 60 mm.

A gap of 5 mm between the foils and the cylinder was used. The tip speed of the rotor was varied, in 2 m/s increments, between 5 m/s and 15 m/s for each rotor tested. The slot velocity was varied at a constant volumetric reject rate of $R_V$ = 0.25 between zero and three meters per second, which was the maximum slot velocity obtainable for the pump without decreasing the feed pressure. The volumetric reject rate is defined as the ratio of the flow that passes into the reject stream and slot velocity $V_S$ is defined as

$$V_S = \frac{Q_A}{A_C} \qquad [4]$$

where $Q_A$ is the volumetric flow rate of the accept stream and $A_C$ is the open area of the cylinder, or the summed cross-sectional area of the slots. It is important to note that the slot velocity is the time average velocity through the slots, not the instantaneous flow velocity. For instance, a slot velocity of $V_S$ = 0 m/s does not mean that there is no instantaneous flow through the slot.
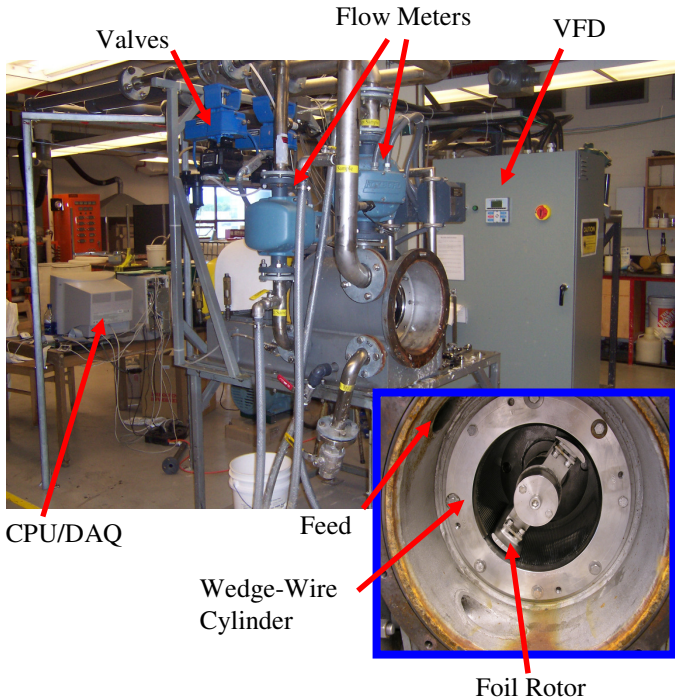


**Figure 3: The MR-8 Laboratory Pressure Screen with Key Components Called Out.**

**Table 1: Test Parameters and Foil Configurations Studied Experimentally.**

| Foil Parameters: | |
|---|---|
| EP and MEF Chord: | 60 mm |
| MEF Angles-of-attack: | 0, 2, 4, 6 deg. |
| MEF Flap Angles: | 12, 17, 22 deg. |
| Clearance Gap: | 5 mm |
| **Cylinder Parameters:** | |
| Cylinder Diameter: | 20.32 cm |
| Cylinder Height: | 22.70 cm |
| Contour Height/Contour Width/Slot Width | 0.9/3.2/0.15 mm |
| **Test Parameters:** | |
| Tip Speeds: | 5, 7, 9, 11, 13, 15 m/s |
| Slot Velocites: | 0, 1, 2, 3 m/s |
| Volumetric Reject Rate: | 0.25 |
| Feed Pressure: | 172.4 kPa |
| Consistency: | 0.0% |

## EXPERIMENTAL RESULTS AND DISCUSSION
### Effect of Tip Speed
The effect of varying tip speed on the pressure pulses generated by the rotor at $V_S$ = 0 m/s is shown in Figure 4 for one of the MEF configurations. Increasing the tip speed increases the magnitude of the pressure pulses generated while maintaining the pulse shape. Similar results were seen for the other MEF configurations and for the EP rotor.

The non-dimensional pressure coefficient, Equation 1, is plotted along the cylinder wall for varying tip speeds in Figure 5 for the same MEF configuration. The traces of pressure coefficient for both rotors collapse into a single curve, showing that, as seen in previous studies (4, 12), the magnitude of the non-dimensional pressure pulse is independent of Reynolds number. Below a tip speed of $V_t$ = 9 m/s, the magnitude of the pressure pulse generated begins to diminish and the dimensionless pressure $C_P$ no longer collapses to a single curve. This is an indication that the flow is beginning to separate from the foil. The same result was seen for the EP rotor below a tip speed of $V_t$ = 11 m/s, as shown in Figure 6, which shows the $C_P$ traces for the EP rotor at various tip speeds.

### Effect of Varying MEF Geometry
The effect of varying the angle-of-attack of the MEF at a constant flap angle on the non-dimensional pressure pulse generated by the foils is shown in Figure 7. Increasing the angle-of-attack of the foil increases the magnitude of the negative pressure pulse and reduces the magnitude of the positive pressure pulse. Similarly, the effect of varying the flap angle of the MEF at a constant angle-of-attack on the pressure pulse is shown in Figure 8. Increasing the flap angle can be seen to also increase the magnitude of the negative pressure pulse.

The effects of varying the MEF geometry are more clearly seen in Figure 9, which shows minimum $C_P$ plotted versus flap angle, with lines of constant angle-of-attack, at different tip speeds. The angle-of-attack is varied from $\alpha$ = 0 deg. to $\alpha$ = 6 deg., and the flap angle is varied from $\delta$ = 12 deg. to $\delta$ = 22 deg. There are clear trends of increasing magnitude of the minimum $C_P$ when increasing both the angle-of-attack and the flap angle, and there is not an optimum for either variable within the range of geometries tested, indicating that lower $C_P$ designs may be possible. Also, the trends do not vary with tip speed. The highest magnitude minimum $C_P$ measured at $V_t$ = 13 m/s was at $(\alpha, \delta)$ = (6, 22), at $C_P$ = -0.81, which is 126% higher in magnitude than measured for the EP rotor. Additionally, it is interesting to note that although the magnitude of the non-dimensional pressure pulses was shown previously in Figure 5 to reduce at tip speeds below $V_t$ = 9 m/s, the trends remain unchanged even at $V_t$ = 7 m/s. This implies that the flow has only partially separated from the foil at this point and the foil is not fully stalled.
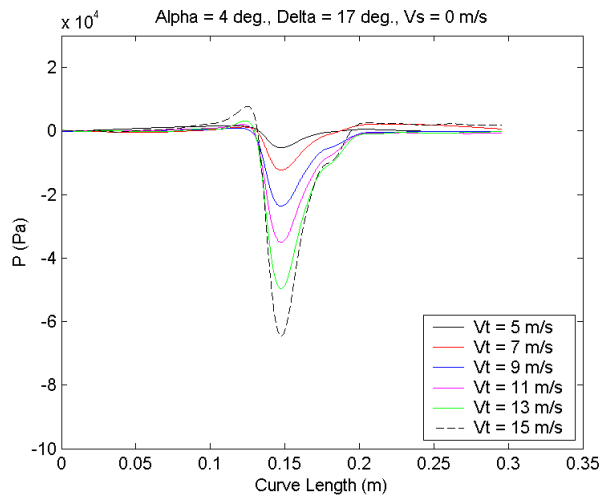
**Figure 4: Pressure Traces for the MEF Rotor at (α, δ) = (4, 17) deg., at Various Tip Speeds, and at V_S = 0 m/s.**



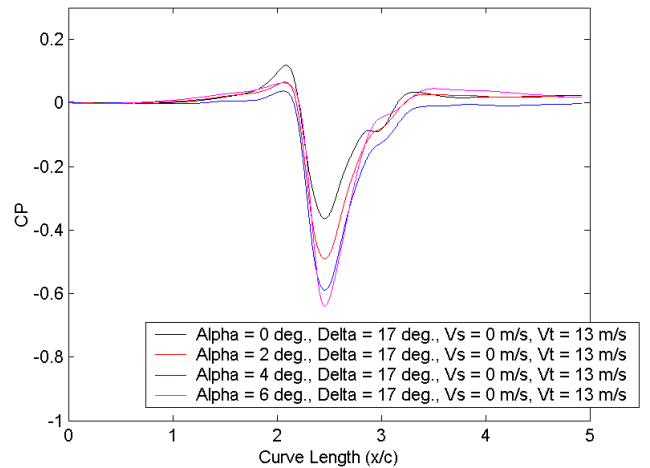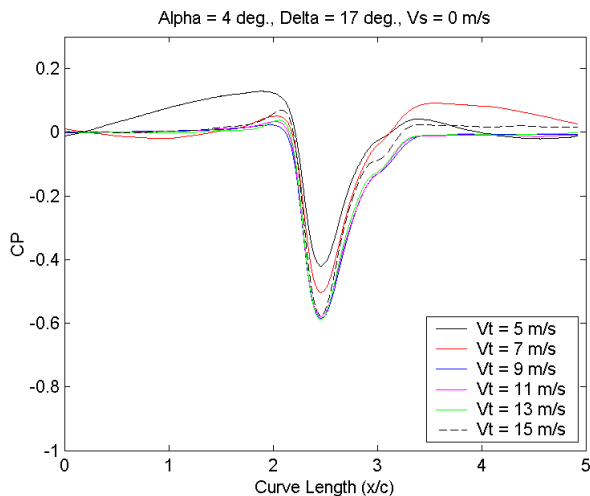**Figure 5: Traces of Non-Dimensional Pressure Coefficient for the MEF Rotor at (α, δ) = (4, 17) deg., at Various Tip Speeds, and at V_S = 0 m/s.**



**Figure 6: Traces of Non-Dimensional Pressure Coefficient for the EP Rotor, at Various Tip Speeds, and at V_S = 0 m/s.**



**Figure 7: Effect of Varying Angle-of-Attack on the Non-Dimensional Pressure Trace for the MEF at a Constant Flap Angle (δ = 17 deg.). The Tip Speed is $V_t$ = 13 m/s and the Slot Velocity is $V_S$ = 0 m/s.**
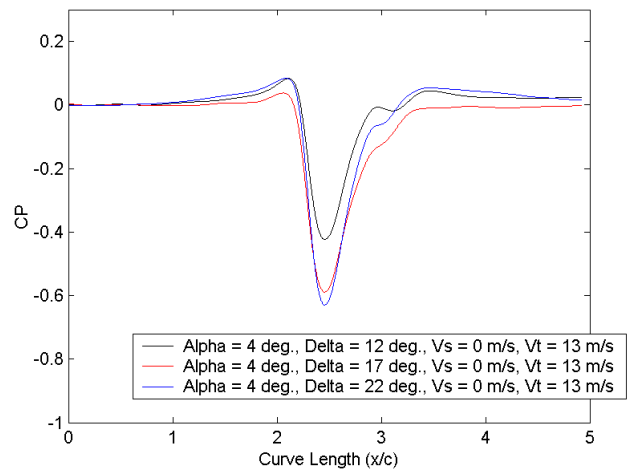


**Figure 8: Effect of Varying Flap Angle on the Non-Dimensional Pressure Trace for the MEF at a Constant Angle-of-Attack (α = 4 deg.). The Tip Speed is $V_t$ = 13 m/s and the Slot Velocity is $V_S$ = 0 m/s.**
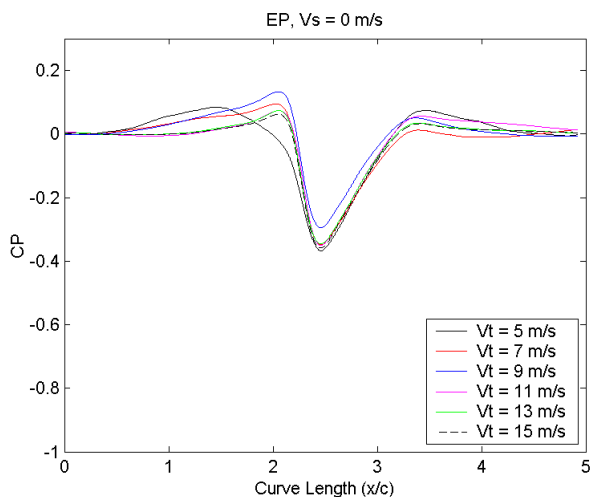
## Effect of Slot Velocity

The effect of increasing the slot velocity on the non-dimensional pressure pulse for a MEF configuration at various tip speeds is shown in Figure 10. At high tip speeds, where the flow around the foil is fully attached, increasing the slot velocity has no effect on the magnitude or shape of the pressure pulse. Increasing slot velocity appears to increase the tip speed at which stall occurs, however. At $V_t$ = 9 m/s, for instance, the pressure pulses for $V_S$ = 0 m/s and $V_S$ = 1 m/s are largely unaffected, but the pressure pulses for slot velocities above $V_S$ = 1 m/s diminish in strength as slot velocity is increased. At $V_t$ = 7 m/s and below, only the pressure pulse at $V_S$ = 0 m/s has retained its shape and magnitude, while the pressure pulses at higher slot velocities have diminished in strength. The large amount of noise in the pressure trace at the higher slot velocities indicates that the flow is likely separated from the foil. Increasing slot velocity likely causes flow separation from the foil at higher tip speeds because of the
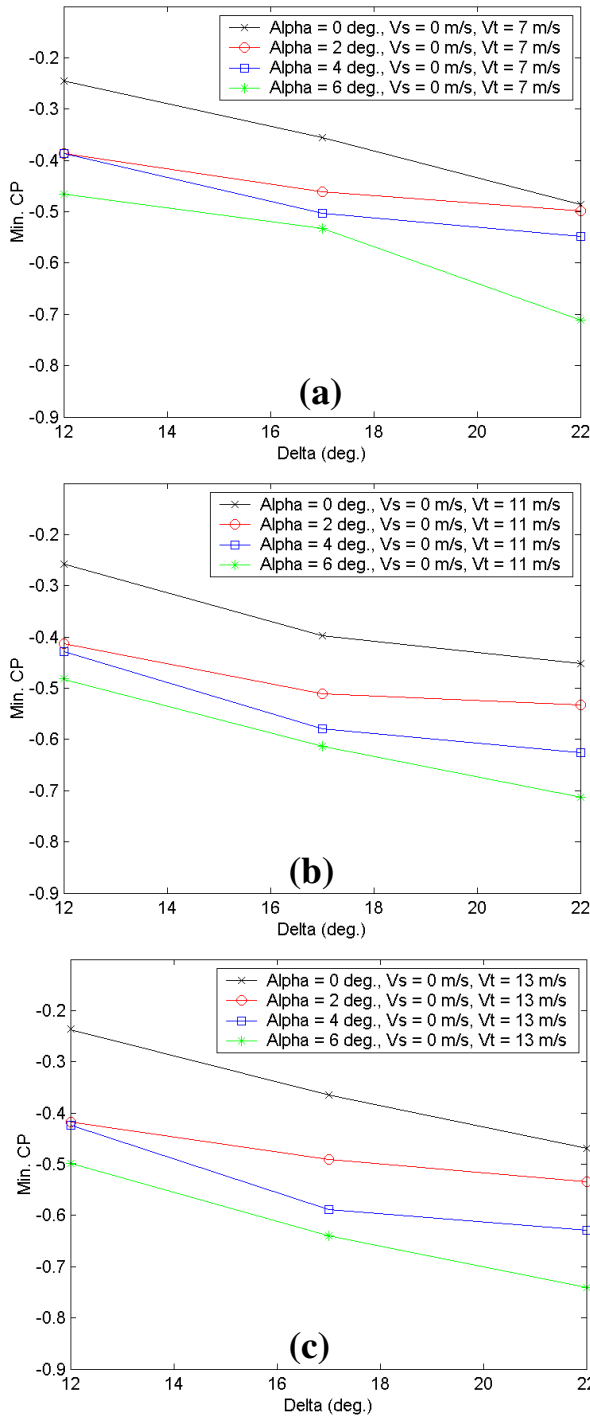
5

*Figure 9: Effect of Varying the MEF Flap Angle on the Minimum Pressure Coefficient, with Lines of Constant Angle-of-Attack, at $V_S$ = 0 m/s and (a) $V_t$ = 7 m/s, (b) $V_t$ = 11 m/s, and (c) $V_t$ = 13 m/s.*



*Figure 10: Effect of Varying Slot Velocity on the Non-Dimensional Pressure Trace for the MEF Rotor at (α, δ) = (2, 17) deg. at (a) $V_t$ = 5 m/s, (b) $V_t$ = 9 m/s, and (c) $V_t$ = 13 m/s.*

increasing adverse pressure gradient associated with it. Similar results were also seen for the single-element EP foil.

This is also seen clearly in Figure 11, which shows the minimum pressure coefficient plotted as a function of slot velocity for the MEF configuration. Increasing slot velocity can be seen to have little effect on the minimum pressure
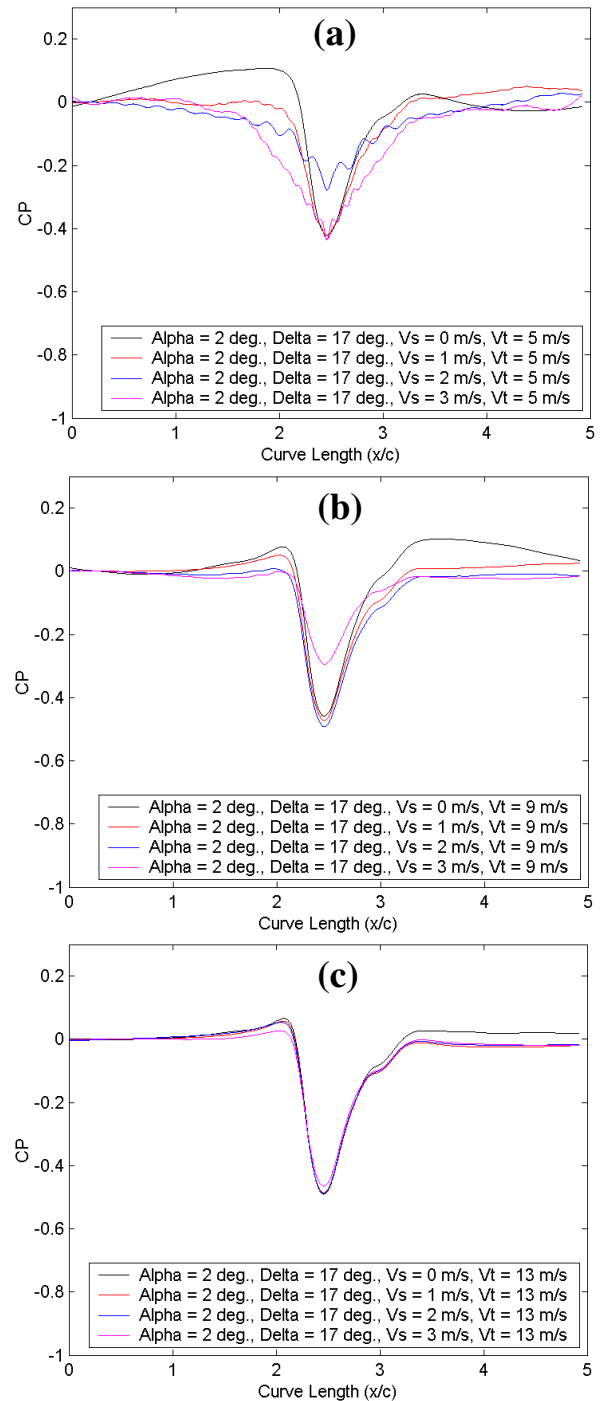
coefficient at higher tip speeds, where the flow is fully attached to the foil. Increasing $V_S$ can again be seen to reduce the tip speed at which flow separation begins, however. This is indicated by the curve for $V_t$ = 9 m/s, which shows a reduction in the magnitude of minimum $C_P$ at $V_S$ = 3 m/s, even though it had been unaffected at the lower slot velocities.

Similar results were seen for the other MEF configurations and for the single-element EP rotor. It was also found that increasing flap angle for the MEF causes the foil to stall at higher tip speeds as slot velocity is increased. This is likely due to the increase in effective camber as the flap angle is increased, which has been shown in previous studies to make the foil more susceptible to flow separation (3, 4). In general, at higher tip speeds, the trends for varying geometry on minimum $C_P$ were unaffected by increasing slot velocity, even at $V_S = 3$ m/s.

## NUMERICAL METHODS

The MEF rotor in the MR8 pressure screen was numerically modeled using the methods described in Delfel *et al.* (19). Figure 12 shows how the domain was modeled, as well as a typical mesh and boundary conditions used in the problem. The discretized Navier-Stokes equations were solved using the FLUENT 6.1 commercial solver, a second order finite volume solver. The problem is assumed to be two-dimensional, isothermal, and steady state. All meshes were generated using GAMBIT, the pre-processing package for FLUENT.

The domain is rotationally periodic, simulating a two-bladed rotor. A rotating coordinate system spinning at the same speed as the rotor is set at the center of the cylinder, since the flow is steady from this frame of reference. Eliminating the time dependence and solving the problem as steady state reduces the computational costs of the problem significantly. The inner wall and the foil were set to have zero velocity relative to the spinning computational coordinate system. The outer wall, which represents the cylinder wall, is set to have zero velocity in the absolute coordinate system.

There are a number of assumptions made in the CFD model, including that the problem is two-dimensional and that there is no flow through the cylinder wall. Typical pressure screen rotors have high aspect ratios and the axial flow velocity is a very low, making the two-dimensional assumption valid. Modeling the cylinder as a solid wall is meant to represent the critical case of a plugged cylinder. It also significantly reduces computational costs by eliminating the need to model the complicated flow through the slots.

Turbulence in the flow was modeled using the standard $k$-$\varepsilon$ model with enhanced wall treatment and the $k$-$\omega$ SST model, and the effectiveness of each was compared. The standard $k$-$\varepsilon$ model finds closure for the Reynolds Stresses by solving additional transport equations for the turbulent kinetic energy $k$ and the turbulent dissipation rate $\varepsilon$. The $k$-$\omega$ SST model is similar to the standard $k$-$\varepsilon$ model, but it instead solves transport equations for $k$ and $\omega$, the ratio of dissipation rate to turbulent kinetic energy, in the near-wall region. Far from the wall, however, it blends the $k$-$\omega$ model into the standard $k$-$\varepsilon$ model. In some cases, the $k$-$\omega$ SST model has been shown to outperform the $k$-$\varepsilon$ model, especially in cases with swirling flows, significant streamline curvature, and adverse pressure gradients (22-25). Additional details of the turbulence models are beyond the scope of this work and are left to the references (23, 26).

Both turbulence models studied require the first mesh point from the foil surface to be at a wall unit of $y^+ = 1$. This required a very fine C-mesh to be used around the foil and in the wake region. A much coarser mesh was used in the far field in order to reduce computational costs, and the two meshes were blended using an unstructured block. A full grid independence study was conducted with geometrically similar meshes spanning 32,000 volumes to 300,000 volumes. The solution was found to be grid independent for meshes over
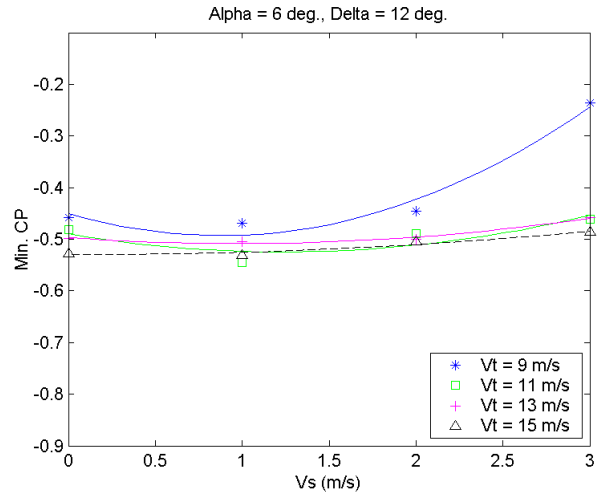


*Figure 11: Minimum Pressure Coefficient as a Function of Slot Velocity for the MEF Rotor at (α, δ) = (6, 12) deg. at Various Tip Speeds.*

*Table 2: Test conditions used in the simulations.*

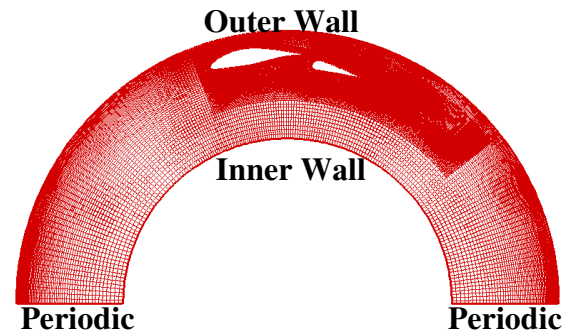| Foil Parameters: | |
|---|---|
| MEF Chord: | 60 mm. |
| Angles-of-attack: | 0, 2, 4, 6 deg. |
| Flap Angles: | 12, 17, 22 deg. |
| Clearance Gap: | 5 mm. |
| **Cylinder Parameters:** | |
| Cylinder Diameter: | 20.32 cm. |
| **Test Parameters:** | |
| Tip Speed: | 20 m/s |
| Fluid: | Water, 20°C |



*Figure 12: Computational Domain Used in the Study and a Typical Mesh with Boundary Conditions Labeled.*

75,000 volumes. The operating conditions used for the simulations are shown in Table 2. The foil chord length, gap, angles-of-attack and flap angles studied are the same as those used in the experiments. The simulations were run at a tip speed of $V_t$ = 20 m/s.

## NUMERICAL RESULTS AND DISCUSSION

Figure 13 shows the experimental and numerical non-dimensional pressure traces for the MEF at $(\alpha, \delta)$ = (0, 22) deg. Changing the turbulence model can be seen to have little effect on the numerical results. Also, for the configuration shown, the numerical results capture the negative portion of the pressure pulse well, but severely under predict the magnitude of the positive pressure pulse. The numerical results for the $k$-$\varepsilon$ model over predict the magnitude of the negative pressure pulse by 5.8%, while the results for the $k$-$\omega$ SST model over predict the magnitude of the negative pressure pulse by 7.3%. Because the $k$-$\varepsilon$ model was shown to have slightly better performance, all numerical results shown and discussed from here on were generated using that turbulence model.

Figure 14 shows minimum pressure coefficient plotted as a function of flap angle with lines of constant angle-of-attack from the CFD results. The results for $\alpha$ = 0 deg. and $(\alpha, \delta)$ = (2, 12) deg. match well with the experimentally measured values. Increasing either angle-of-attack or flap angle beyond $(\alpha, \delta)$ = (2, 12) deg. causes a reduction in the magnitude of the minimum pressure coefficient, with an optimum value at $(\alpha, \delta)$ = (0, 22) deg. This is significantly different than what was shown experimentally, where the magnitude of the minimum pressure coefficient continued to increase as angle-of-attack and flap angle were increased.

The reduction of the magnitude of the negative pressure pulse as the angle-of-attack and flap angle are increased beyond an optimum value is likely due the flow separating from the foil. This was described in Delfel et al. (19) and is also shown in Figure 15, which shows pressure contours and streamlines for the MEF at varying angles-of-attack and a constant flap angle. As the angle-of-attack is increased beyond $\alpha$ = 2 deg., the main foil begins to stall, reducing the magnitude of the negative pressure pulse. The reason that the simulations predict flow separation well before what was found experimentally is likely due to use of a solid wall boundary condition rather than the actual slotted screen cylinder. If the flow through the slots had been simulated, momentum would have been transferred through the slots as they were backflushed, preventing flow separation over the foil.

The use of the solid wall rather than modeling the flow through the slots therefore makes the simulations overly conservative in the predicting the angles for the optimum MEF configuration – the experimental results show that the MEF can be operated at higher angles without stalling the foil. While this limits the effectiveness of the model used, it is still been shown to be a useful tool, since the MEF was designed using this model and has been shown to perform well in pilot plant and full scale mill trials (20, 21). The results from the numerical model may also provide insight into how the
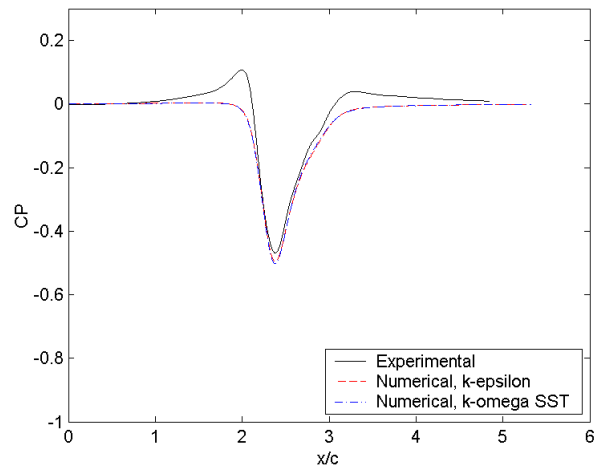


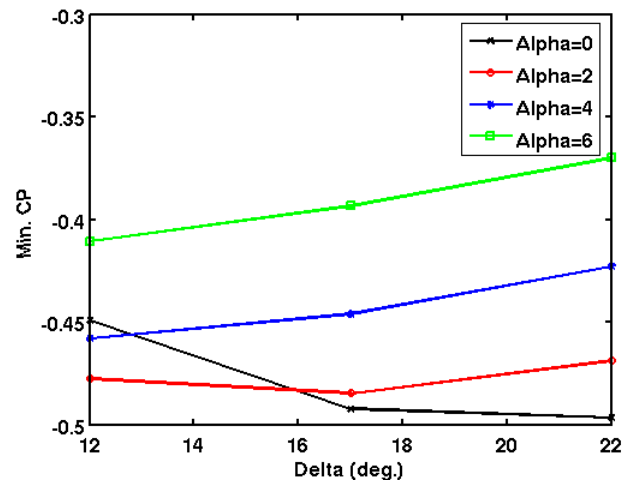**Figure 13: Experimental and Numerical Non-Dimensional Pressure Traces for the MEF at (α, δ) = (0, 22) deg.**



**Figure 14: Numerically Predicted Minimum Pressure Coefficient on the Cylinder Wall for Varying MEF Geometry. The Results Were Obtained Using the k-ε Turbulence Model.**

optimum configuration of the rotor changes as the cylinder blinds. As the cylinder blinds, the numerical results suggest that the MEF at higher angles-of-attack would stall and cause the screen to fail suddenly, but the MEF at lower angles-of-attack would not be as strongly affected. Further analysis, both experimentally and numerically, is needed to fully understand these phenomena, however.

As mentioned previously and shown in Figure 13, the model under predicts the magnitude of the maximum pressure coefficient by an order of magnitude compared to the experimental results. The reason that the CFD under predicts the magnitude of the maximum pressure coefficient is again likely due to the use of a solid wall boundary rather than a slotted cylinder. With a slotted cylinder, the adverse pressure gradient across the slots would likely cause the stagnation point at the leading edge of the foil to be further towards the upper surface of the foil (closer to the cylinder) than in the

Copyright © 2010 by ASME

case of a solid cylinder wall. As discussed in other studies, this would cause the positive pressure pulse transmitted from the foil to screen wall to be stronger (1, 3, 4, 19).

## CONCLUSIONS

The pressure pulses produced by a multi-element foil rotor and a single-element foil rotor were studied experimentally in a laboratory pressure screen. The effects of foil angle-of-attack, flap angle, rotor tip speed and flow rates on pressure pulse magnitude and shape were determined.

It was shown that at high enough tip speeds, the non-dimensional pressure pulse is Reynolds number independent, and that the magnitude of the pressure pulse varies with rotor tip speed squared. At low tip speeds the magnitude of the non-dimensional pressure pulse begins to fluctuate and diminish, most likely because of the onset of separation of the flow over the foils.

It was also shown that increasing both the angle-of-attack and the flap angle of the MEF increases the magnitude of the negative pressure pulse. The best MEF configuration in terms of the magnitude of the negative pressure pulse was at $(\alpha, \delta) = (6, 22)$ deg., generating a peak negative pressure coefficient of $C_P = -0.81$, which was a 126% increase in magnitude compared to the single-element foil. Increasing the angle-of-attack and the flap angle also reduced the magnitude of the positive portion of the pressure pulse until an optimal angle, beyond which the magnitude of the positive pulse increased. The best performing MEF configuration with respect to the positive pulse reduced the magnitude of the maximum $C_P$ by 39% compared to the single-element foil rotor.

Increasing the slot velocity was shown to have no effect on the magnitude of the pressure pulses or the trends for varying geometry above a critical tip speed. The critical tip speed at which the pressure pulse caused by the foil becomes Reynolds number independent was found to increase with increasing slot velocity. This is most likely due to the increase in adverse pressure gradient associated, which leads to flow separation at lower Reynolds numbers.

Finally, the results of a CFD model of the MEF rotor in a pressure screen were compared to the experimental results. For low angles-of-attack, the simulations predicted the negative portion of the pressure pulse well, but significantly under predicted the magnitude of the positive pulse. The CFD model also predicted the foil would begin to stall above an angle-of-attack of $\alpha = 2$ deg., causing the magnitude of the negative pressure pulse to diminish. This caused the simulations to under predict the magnitude of the negative pressure pulse at higher angles of attack. It is likely that the simulations over predicted flow separation due to the use of a solid wall as the screen cylinder, which was meant to represent a plugged cylinder. In reality, low momentum fluid is transferred to the foils as the slots are backflushed, preventing stall. In spite of these limitations, the CFD model has been shown to provide insight into the flow physics and to be a useful design tool for pressure screen rotors.
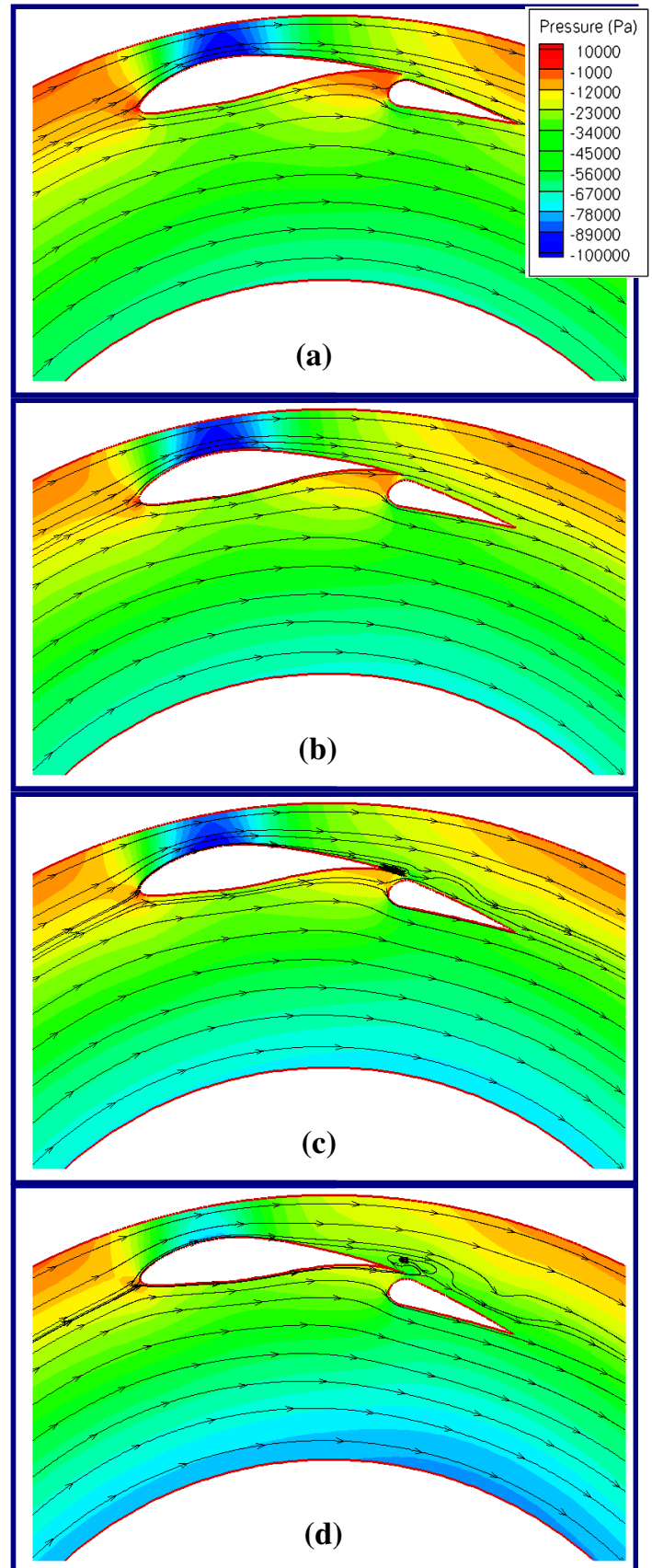


**Figure 15: Numerically Generated Pressure Contours and Streamlines for the MEF at (a) α = 0 deg., (b) α = 2 deg., (c) α = 4 deg., and (d) α =6 deg., and a Flap Angle of δ = 12 deg.**

9

**REFERENCES**

1. Feng, M., "Numerical Simulation of the pressure pulses generated by a pressure screen foil rotor", M.A.Sc. Thesis, Dept. Mech. Eng., Univ. British Columbia, 2003.

2. Feng, M., Olson, J.A., Ollivier-Gooch, C.F., Xia, J., and Gooding, R.W., A computational fluid dynamic (CFD) tool for advanced pulp screen foil rotor design", 2003 ABTCP Conf.

3. Feng., M., Gonzales, J., Olson, J.A., Ollivier-Gooch, C., and Gooding, R.W., "Numerical simulation of the pressure pulses produced by a pressure screen foil rotor", J. Fluid Eng., 127(2):347-357 (2005).

4. Gonzales, J., "Characterization of design parameters for a free foil rotor in a pressure screen", M.A.Sc. Thesis, Dept. Mech. Eng., Univ. British Columbia, 2002.

5. Pflueger, C.D., Olson, J.A., and Gooding, R.W., "The performance of the EP Rotor in de-ink pulp screening", 2007 Appita Conf., 165-169.

6. Niinimaki, J., "Phenomena affecting the efficiency of a pressure screen", 1999 Tappi Pulping Conf., 957-966.

7. Julien Saint Amand, F., and Perrin, B., "Fundamentals of screening: Effect of rotor design and fibre properties", 1999 Tappi Pulping Conf., 941-955.

8. Julien Saint Amand, F., and Perrin, B., "Basic parameters affecting screening efficiency and fibre loss", 2000 PTS-CTP Deinking Symposium, 26.1–26.22.

9. Wakelin, R.F., Blackwell, B.G., and Corson, S.R., "The influence of equipment and process variables on mechanical pulp fractionation in pressure screens", 1994 Appita Conf., 611-621.

10. Wakelin, R.F., and Corson, S.R., "TMP long fractionation with pressure screens", 1995 Int. Mech. Pulping Conf., 257-265.

11. Wakelin, R.F., and Corson, S.R., "Reject thickening behavior of TMP screening", Pulp Paper Can., 99(1): 27-30, 1998.

12. Pinon, V., Gooding, R.W., Olson, J.A., "Measurement of pressure pulses from a solid core rotor", Tappi J., 2(10): 9-12, 2003.

13. Olson, J.A., Turcotte, S., Gooding., R.W., "Determination of power requirements for solid core pulp screen rotors", Nordic Pulp Paper Res. J., 19(2):213-217, 2004.

14. Yu, C.J., "Pulsation measurement in a screen. Part I: Pulse signature and magnitude of S-shape rotor", 1994 Tappi Engineering Conf., 767-782.

15. Atkins, M., "Axial variations and entry effects in a pressure screen", Ph. D. Thesis, Dept. of Eng., Univ. of Waikato, 2007.

16. Karvinen, R., and Halonen, L., "The effect of various factors on pressure pulsation of a screen", Paperi ja Puu, 2: 80-83, 1984.

17. Wikstrom, T., and Fredriksson, B., "Hydrodynamics in a pressure screen – consequences on the separation process", 5th Research Forum on Recycling Preprints, 1999, 197-202.

18. Luukonen, A., Delfel, S., Olson, J.,Pflueger, P., and Ollivier-Gooch, C., "Numerical simulations of pressure pulses produced by a solid core pressure screen rotor", 2007 Appita Conf., 265-271.

19. Delfel, S., Ollivier-Gooch, C., and Olson, J., "A numerical investigation into the effectiveness of multi-element pressure screen rotor foils", J. Fluid Eng., 131(1): 011101-1, 2009.

20. Olson, J.A., Pflueger, C., Delfel, S., Ollivier-Gooch, C.F., Martin, P., Vaulot, F., and Gooding, R., "High Performance Foil Rotor Improves De-Ink Pulp Screening", Progress in Paper Recycling, 2009 (?).

21. Hamelin, M., Delfel, S., Olson, J., and Ollivier-Gooch, C., "High performance multi-element foil (MEF) pulp screen rotor – pilot and mill trials", 2009 Paptac Conf. preprints.

22. Naser, J.A., "Prediction of Newtonian and non-Newtonian flow through concentric annulus with centerbody rotation", Int. Conf. on CFD in Mineral and Metal Proc. and Power Generation Proc., CSIRO, Melbourne, 273-278, 1997.

23. Wilcox, D.C., "Turbulence modeling for CFD", California, USA, DWC Industries, Inc., 1998.

24. Menter, F.R., "Performance of popular turbulence models for attached and separated adverse pressure gradient flows", AIAA J., 30(8): 2066-2072, 1992.

25. Menter, F.R., "2-Equation eddy-viscosity turbulence models for engineering applications", AIAA J., 32(8): 1598-1605, 1994.

26. Pope, S.B., "Turbulent Flows", Cambridge Press, 2000.